Atmospheric
Measurement
Techniques
Discussions

Quantitative comparison of measured and simulated O$_4$ absorptions for one day with extremely low aerosol load over the tropical Atlantic

Thomas Wagner[1], Steffen Dörner[1], Steffen Beirle[1], Sebastian Donner[1], Stefan Kinne[2]

[1]Satellite Remote Sensing Group, Max Planck Institute for Chemistry, Mainz, Germany
[2]Max-Planck Institute for Meteorology, Hamburg, Germany

Correspondence to: Thomas Wagner (thomas.wagner@mpic.de)

Abstract. In this study we compare measured and simulated O$_4$ absorptions for conditions of extremely low aerosol optical depth (between 0.034 to 0.056 at 360nm) on one day during a ship cruise in the tropical Atlantic. For such conditions, the uncertainties related to imperfect knowledge of aerosol properties don't significantly affect the comparison results. We find that the simulations underestimate the measurements by 15% to 20%. Even for simulations without any aerosols the measured O$_4$ absorptions are still systematically higher than the simulation results. The observed discrepancies can not be explained by uncertainties of the measurements and simulations and thus indicate a fundamental inconsistency between simulations and measurements.

1 Introduction

Remote sensing measurements of the atmospheric absorption of the oxygen dimer $(O_2)_2$ are often used to derive properties of aerosols and clouds. The atmospheric concentration of $(O_2)_2$ (in the following referred to as O$_4$) varies only slightly with temperature, pressure and humidity variations (aside the dependence on altitude). Thus deviations from the O$_4$ absorptions for clear sky conditions indicate changes of the atmospheric radiative transfer, e.g. due to clouds and aerosols. In recent years, inconsistencies between the measured atmospheric O$_4$ absorption and radiative transfer simulations were detected for Multi-AXis-DOAS (MAX-DOAS) observations. MAX-DOAS instruments measure scattered sun light under different, mostly slant elevation angles (Hönninger and Platt, 2002). Several studies found that a scaling factor (SF<1) had to be applied to the observed atmospheric O$_4$ absorptions in order to bring them into agreement with radiative transfer simulations. Other studies, however, did not find the need to apply such a scaling factor (e.g. Ortega et al., 2016; see also discussion in Wagner et al., 2019, and references therein). One major difficulty in the quantitative interpretation of these comparisons is that usually the atmospheric aerosol properties are not well known (e.g. the vertical extinction profile and/or the optical properties). And even if they were known, it is still a challenge to accurately represent them in atmospheric radiative transfer simulations.

In this study we mainly minimise these difficulties by using atmospheric observations in the presence of very low aerosol loads. During a ship campaign across the tropical Atlantic, very low aerosol optical depth (AOD) was observed on one day (2 May 2019). At 360 nm (the wavelength at which we analyse the atmospheric O$_4$ absorption), the AOD ranged from 0.034 to 0.056, which is an order of magnitude lower than the optical depth of molecular Rayleigh scattering.

Like in previous studies, we compare the observed atmospheric O$_4$ absorption with the results of radiative transfer simulations. Information about the aerosol properties is derived from sun photometer measurements in combination with ceilometer measurements. Also in our study, considerable uncertainties about the aerosol vertical profile and the aerosol optical properties exist. However, these uncertainties are less important for the interpretation of the comparison results than in previous studies because of the low AOD, and we find large discrepancies between the measured and simulated O$_4$ absorptions.

The paper is organised as follows: In section 2, an overview on the ship campaign and the instruments used in this study is given. Sections 3 to 5 describe the spectral analysis, the cloud classification, and the calculation of the O$_4$ profile. In section

6, the radiative transfer simulations and the extraction of the aerosol extinction profiles are presented. Section 7 presents the comparison results, and section 8 the summary and conclusions.

2 Overview on the ship campaign and the instruments used in this study

The MAX-DOAS measurements were carried out during a cruise (MSM82/2) of the German research vessel RV Maria S. Merian (https://www.ldf.uni-hamburg.de/merian.html) from Montevideo (Uruguay) to Las Palmas (Spain) from 26 April 2019 to 14 May 2019 (see Fig. 1). More details on the ship cruise MSM82/2 can be found in Krastel et al. (2019). In this study, we focus on one day with particularly low AOD (2nd May), which is marked in Fig. 1.

The MAX-DOAS instrument was mounted above the ship's bridge at about 20m altitude above sea level. The telescope was aligned in the driving direction of the ship (Fig. 2).

2.1 MAX-DOAS instrument

The MAX-DOAS instrument is a so-called Tube MAX-DOAS instrument which was developed and built by the electronic workshop of the Max Planck Institute for Chemistry in Mainz (Donner, 2016). It consists of two major parts: the telescope unit and the spectrometer unit. The telescope unit is mounted outside on the railing of the ship. The spectrometer unit is located inside the ship. Besides the spectrometer it also contains a peltier cooling element which stabilises the spectrometer temperature at 15 °C. Both units are connected via a quartz glass fibre bundle and electric cables. The telescope unit is equipped with a gyroscope to stabilise the elevation angles by continuously adjusting the motor position with an accuracy of ±0.1°.

The spectrometer is an Avantes ULS2048x64-USB2. It covers the spectral range from 299.4 nm to 463.1 nm with a spectral resolution between 0.52 and 0.54 nm as described by the full width half maximum (FWHM). Spectra are measured with an integration time of 1 min at the following elevation angles: -2°, -1°, -0.5°, 0°, 0.5°, 1°, 2°, 3°, 4°, 5°, 6°, 8°, 10°, 15°, 30°, 90°. Note that in this study only measurements with positive elevation angles are used. One elevation sequence is completed within about 21 min. Dark current and offset spectra are taken during night and are used to correct the measured spectra before the spectral analysis.

2.2 Sun photometer

A MICROTOPS II sunphotometer provided atmospheric totals on aerosol and water vapor. The instrument, when directed towards the sun (in a handheld operation), captures via diodes the solar intensity in five sub-spectral bands near wavelengths of 380, 440, 670, 870 and 940nm. In combination with the larger reference solar intensity at the top of the atmosphere - using time and (GPS-provided) position data - sun-photometer measurements define the atmospheric attenuation at these solar sub-spectral bands. Four spectral bands (near 380, 440, 670 and 870 nm) sample in trace-gas poor regions, while one spectral band (near 940nm) is strongly affected by water vapor absorption. In the absence of clouds, the solar attenuations in the four trace-gas poor bands can be linked to aerosol - after (surface air pressure defined) contributions from air-molecule (Rayleigh) scattering have been removed. Hereby, the aerosol associated attenuations are quantified by the (vertically normalized) aerosol optical depth (AOD). As the instrument offers AOD values simultaneously at four different solar wavelengths, the typical aerosol particle size is revealed and even AOD contributions from sub-micrometer (mainly from pollution and wildfire) and super-micrometer size aerosol particles (mainly from dust and seasalt) can be distinguished. The determination of the atmospheric water vapor is based on the differential absorption between 870 and 940 nm attenuation data. Any quality measurement usually relies on many repeated samples in order to identify and remove poor data associated

with sun-view contamination by clouds and/or inaccurate orientations of the instrument into the sun (with is done manually with the help of a pointing device). NASA's Aeronet sub-group of the Maritime Aerosol Network (MAN, Smirnov et al., 2009) provided the calibrated instrument for the cruise and also stores cruise data at

90 https://aeronet.gsfc.nasa.gov/new_web/cruises_new/Maria_Merian_19_0.html.

2.3 Ceilometer

The Jenoptik 15K ceilometer of the MPI-M is a simple laser system operating at 1064nm, at an invisible trace-gas free near-

95 IR wavelength. Laser impulses are sent upward into the atmosphere and based on strength and delay of backscattered return signals altitude positions for atmospheric aerosol and clouds are derived. Due to their stronger backscatter at optically thicker media, such as clouds, overhead cloud base altitudes are well captured. However, as laser light strongly attenuates in optically thicker media, no information above a cloud base is possible. Vertical profiles of aerosol for clouds-free views (and below clouds) are possible up to about 7km in altitude during the night but only up to about 4km in altitude during the day,

100 due to scattering noise by sunlight. No useful aerosol profiling is possible near the surface (e.g. lower 300m), because signal sender and receiver are not the identical location. Recorded ceilometer data of the cruise are accessible via an anonymous ftp-site at ftp://ftp-projects.zmaw.de/aerocom/ships/ceilometer_MSM/.

3 Spectral analysis

105

The spectral analysis is performed following the settings suggested by Wagner et al. (2019). The spectral range from 352 to 387 nm is chosen, which contains two O_4 absorption bands. The details of the analysis are given in Table 1. Fig. A1 (left) presents an example of the spectral analysis as used in this study. In addition to the other cross sections, also a H_2O cross section (Polyansky et al. 2018) is included. The reason for including a H_2O cross section as well as the effect of including a

110 second O_4 cross section are discussed in appendix A1.

The results of the spectral analysis represent the integrated trace gas concentration along the atmospheric light path, the so-called slant column density (SCD). For O_4 the SCD is expressed with respect to the square of the O_2 concentration (see Greenblatt et al., 1990). Thus, the unit of the O_4 SCD is $molec^2/cm^5$. For the analysis of the measured spectra, a so-called Fraunhofer reference spectrum is used. In this study, the Fraunhofer reference spectrum is calculated as the average of the

115 zenith spectra before and after the chosen elevation sequence, weighted by the time of the selected measurement from that elevation sequence. Before performing the spectral analysis, these sequential Fraunhofer reference spectra are fitted to a 'universal' Fraunhofer reference spectrum (29 April 13:43, SZA: 44.8°, elevation angle: 90°) to transfer the spectral calibration of the universal Fraunhofer reference spectrum to the sequential Fraunhofer reference spectra. The universal Fraunhofer reference spectrum was calibrated using a high resolved solar spectrum.

120 Since the Fraunhofer reference spectrum also contains atmospheric trace gas absorptions, the output of the spectral analysis represents the difference between the SCDs of the selected non-zenith spectrum and the Fraunhofer reference spectrum, the so-called differential SCD (or dSCD).

The typical fit error of the derived O_4 dSCD is between $2 \cdot 10^{41}$ $molec^2/cm^5$ and $4 \cdot 10^{41}$ $molec^2/cm^5$. Depending on the magnitude of the retrieved O_4 dSCD this corresponds to relative errors between 1 and 4 %.

125

4 Cloud detection using the MAX-DOAS measurements

Although during most of the afternoon on 2 May clear sky conditions prevailed, also some scattered clouds were present. They were e.g. detected by the ceilometer in zenith direction (see Fig. 3). In order to derive information about possible cloud

130 contamination for the individual MAX-DOAS measurements, the MAX-DOAS measurements themselves were used for the detection of cloud contamination, similar as in Wagner et al., (2014, 2016). Figure A3 in the appendix shows the time series of the retrieved O_4 dSCDs on 2 May for the different elevation angles. During the morning the O_4 dSCDs show strong variability caused by the presence and variability of clouds as also seen in the ceilometer data (Fig. 3). During the afternoon, for most of the time, smooth variations of the O_4 dSCDs are found indicating clear sky conditions. However, for some times

135 and elevation angles, also small systematic deviations (usually reductions) of the O_4 dSCDs occur, which are caused by scattered clouds. During periods without any cloud contamination, the temporal variability of the retrieved O_4 dSCDs is rather small (scatter of the O_4 dSCDs is typically $\leq 5 \cdot 10^{41}$ molec^2/cm^5). Measurements with deviations $> 10^{42}$ molec^2/cm^5 compared to the extrapolated O_4 SCDs from the smooth (cloud-free) neighboring measurements are thus flagged as cloud-contaminated. From the selected 11 elevation sequences during the mainly cloud-free periods in the afternoon of 2 May, 7

140 are found to be completely free of cloud contamination.

5 Calculation of the O_4 profile and O_4 VCD

The O_4 height profile and VCD for 2 May 2019 are calculated from vertical profiles of temperature and pressure. Also the

145 effect of the atmospheric humidity is accounted for. For the profiles of temperature, pressure and atmospheric humidity we used the results from the ECMWF ERA-Interim data set (Berrisford et al., 2011) for 2 May 2019. From the temperature and pressure profiles the air concentration [air] is calculated. Then the O_2 concentration [O_2] is derived according to the following equation:

150
$$[O_2] = [air] \cdot M_{O2} \cdot (1 - M_{H2O}) \tag{1}$$

Here M_{H2O} is the mixing ratio of water vapour taken from the ERA interim data. For the mixing ratio of O_2 (M_{O2}) a value of 21% is assumed. The O_4 concentration is then represented by the square of the O_2 concentration (Greenblatt et al., 1990). To derive the O_4 VCD, the O_4 concentration is vertically integrated between the surface and 30 km with a vertical resolution of

155 20 m.

The temperature and pressure from the ECMWF ERA-Interim data set at the surface are also compared to the in situ measurements on the ship. It is found that the ECMWF temperature is slightly lower (-0.7 K) and the ECMWF pressure is slightly higher (+2 hPa) than the corresponding in situ measurements, see Fig. A4 in the appendix. Therefore, we repeated our calculations of the O_4 profiles by shifting the ECMWF values for the whole profiles by +0.7 K and – 2 hPa. The

160 resulting change of the O_4 VCD is rather small (+0.3 %). The derived O_4 VCD for the modified profile is (1.245 ± 0.25) $\cdot 10^{43}$ molec^2/cm^5.

To estimate the uncertainty of the derived O_4 VCD the temperature and pressure of the whole profiles are varied by ± 2 K and ± 2 hPa, respectively. The resulting changes of the O_4 VCDs are ± 1.5 % and ± 0.9 %, respectively. In addition, assuming an uncertainty of the atmospheric humidity profile of 30% leads to an uncertainty of the derived O_4 VCD of 0.9 %. Thus, we

165 estimate the total uncertainty of the O_4 VCD to ± 2 %.

Finally, a subtle detail should be mentioned: the integration of the O_4 VCD was performed starting from sea level, while the instrument was located about 20 m above sea level. This rather small difference would result in a reduction of the O_4 VCD by 0.4 %. However, this effect is considered in exactly the same way in the radiative transfer simulations, where the instrument was also put at an altitude of 20 m, while the O_4 AMFs are calculated for the O_4 column starting from sea level.

170 Thus it is a consistent procedure to use the O_4 VCD integrated from sea level for the conversion of the measured O_4 dSCDs into O_4 dAMFs.

Atmospheric
Measurement
Techniques
Discussions

6 Radiative transfer simulations

175   O_4 dSCDs are calculated using the full spherical Monte Carlo radiative transfer model MCARTIM (Deutschmann et al. 2011). For the simulations the profiles of temperature, pressure, and O_4 as described in section 5 are used. The vertical resolution was set to 20 m close to the surface and increases with altitude (see Table 2). The surface albedo was set to 0.05. The simulations were performed for the exact SZA and relative azimuth angles of the individual measurements. From the obtained O_4 AMFs, the corresponding O_4 dAMFs are calculated by subtracting the simulated O_4 AMFs for the zenith

180   viewing direction. To achieve best consistency with the measurements, for the simulation of the zenith measurements (interpolated between the zenith observations before and after the sequence) the SZA and relative azimuth angle for the exact time of the non-zenith measurements are also used for the simulations of the zenith measurements. The temporal evolution of the SZA and relative azimuth angle for 2 May are shown in Fig. A5 in the appendix.

It should be noted that it is important to use a consistent treatment of the SZA and relative azimuth angles in the simulations

185   and measurement analyses. Especially the choice of the Fraunhofer reference spectra is important. If e.g. either zenith measurements before or after the selected elevation sequence are used as reference spectra, systematic deviations of the retrieved O_4 dSCDs of up to 10% can occur (see Fig. A6 in the appendix).

O_4 dAMFs are simulated for two aerosol extinction profiles as well as for a pure Rayleigh atmosphere. For the extraction of the aerosol extinction profiles, the observations by the sun photometer and the ceilometer were used (see section 6.1). For the

190   simulations including aerosols, the phase function is represented by a Henyey-Greenstein (HG) parameterisation with an asymmetry parameter of 0.68. The single scattering albedo was set to 0.95. Variations of these properties lead to changes of the simulated O_4 dSCDs by up to ±3 % (see Fig. A7 in the appendix). These rather low uncertainties are related to the low AOD on 2 May 2019. For measurements with higher aerosol loads, the corresponding uncertainties are usually much larger (e.g. Wagner et al., 2019). Here it should be noted that the HG phase function model is a rather simplified approximation for

195   true aerosol phase functions. Thus especially for measurements with small scattering angles (e.g. around noon on 2 May 2019) the uncertainties of the RTM simulations might be larger.

6.1 Extraction of the aerosol extinction profiles

200   Figure 4 presents the hourly averaged and range corrected ceilometer backscatter profiles for three periods in the afternoon on 2 May 2019 without cloud contamination. In a first order approximation, these backscatter profiles are proportional to the aerosol extinction. Thus together with the total AOD from the sun photometer measurements, the aerosol extinction profiles can be determined. However, ceilometer measurements are affected by several instrumental limitations, which complicate the direct conversion to aerosol extinction profiles:

205   a) Due to the missing overlap between the outgoing beam and the field of view of the detector, the sensitivity of the ceilometer is very low for altitudes below 500 m. Thus for this altitude range, no information on the aerosol extinction can be derived from the ceilometer measurements.

b) In spite of the long averaging period, still strong noise appears for altitudes above 3 km.

Due to these limitations, the ceilometer profiles can only be used for a restricted altitude range. In the following we used the

210   ceilometer profiles for the altitude range between 500 m and about 7 to 9 km. Between 500 m and 3000 m, averages for 100 m layers are calculated. Below 500 m, the values at 500 m are either set constant for the layer below, or are linearly extrapolated from the ceilometer data between 500 m and 800 m (similar as in Wagner et al., 2019). Since between 3 km and 10 km the noise increases strongly, a third order polynomial was fitted to the ceilometer data in that height range. The polynomial values are used for the altitude range for which positive values are obtained. Between 7 and 9 km the polynomial

215   values for the three profiles cross zero. Above these altitudes, the the profile values are set to zero. These extraction steps are illustrated in Fig. A8 in the appendix.

Before the backscatter profiles are normalised with the total AODs measured by the sun photometer, the stratospheric part of the total aerosol profile has to be added. This step is usually not important, because in more polluted areas the total AOD is clearly dominated by the tropospheric part. However, for our study, the total AOD is so low that the stratospheric part

220   constitutes a substantial fraction (up to 25 %) of the total AOD. Thomason et al. (2018) report the stratospheric AODs in the Tropics at 525 nm to be about 0.005 to 0.006. Assuming an Angström exponent of 2 the corresponding AOD at 360 nm is estimated to around 0.011 and 0.013. In the following we used a value of 0.012.

This value is subtracted from the total AOD (Fig. 3) measured by the sun photometer. Then the tropospheric aerosol profiles (as decsribed above, see also Fig. A8) are normalised by the resulting tropospheric AOD. Finally, the stratospheric extinction

225   profile is added to the normalised tropospheric aerosol extinction profiles. For the stratospheric extinction profile we used a simplified shape with an AOD of 0.012. Here it is important to note that the details of the extinction profile in the upper troposphere and stratosphere are not critical. For example, the simulated O_4 dAMFs using aerosol profiles with or without the stratospheric part are almost the same. The final aerosol extinction profiles used for the RTM simulations are shown in Fig. 4.

230

6.2 Calculation of effective temperatures for the O_4 absorption

Since the temperature of the troposphere decreases with altitude, and the O_4 absorption cross section depends on temperature, the retrieved O_4 dSCDs might deviate from the true O_4 dSCDs (the integrated O_4 concentration along the

235   atmospheric light paths), because only one O_4 cross section for a fixed temperature is used in the spectral analysis. Thus, before the O_4 dAMFs from the measured spectra are compared to those from the radiative transfer simulations, the effect of the temperature dependence of the O_4 absorption has to be investigated.

The effective temperature of the O_4 measurements is calculated according to:

240
$$T_{eff,\alpha} = \frac{\sum_z [O_4]_z \cdot (bAMF_{z,\alpha} - bAMF_{z,90°}) \cdot T_z}{\sum_z [O_4]_z \cdot (bAMF_{z,\alpha} - bAMF_{z,90°})}$$
(2)

Here $[O_4]_z$ represents the O_4 concentration at altitude z, $bAMF_{z,\alpha}$ the box-AMF for elevation angle α at altitude z, and T_z the temperature at altitude z. $T_{eff,\alpha}$ is the effective temperature for the measured O_4 dSCD at elevation angle α.

Equation 2 is applied for each individual measurement, the results are shown in Fig. A9. The effective temperatures range

245   from 276 K to 299 K. They depend systematically on the elevation angle and SZA. Measurements at low elevation angles are most sensitive for the layers near the surface, at which the highest temperatures occur. Measurements at high SZA (towards the end of the considered time period) have higher sensitivities for higher atmospheric layers with colder temperatures. Both dependencies are well represented by the results shown in Fig. A9.

To correct the effect of the temperature dependence, the correction factors presented in Fig. 13 in Wagner et al. (2019) are

250   applied to the O_4 dSCDs retrieved with the O_4 cross section for 293 K. The corrected O_4 dSCDs differ by up to a few percent (between –2 % and +7 %) from the original O_4 dSCDs. In Fig. A10 in the appendix the effect of the temperature correction is shown for two selected elevation sequences. For the comparison with the radiative transfer simulations the temperature-corrected O_4 dSCDs (or dAMFs) are used.

255   **7 Comparison results**

Atmospheric
Measurement
Techniques
Discussions
EGU

7.1 Direct comparison between measurements and RTM results

In Fig. 6 the O_4 dAMFs derived from the MAX-DOAS measurements are compared to those obtained from the radiative

260   transfer simulations for elevation sequences not affected by clouds (similar comparisons for the sequences with cloud-contaminated measurements are shown in Fig. A11 in the appendix).

In the left part of Fig. 6, the results from radiative transfer simulations without aerosols are shown. Here, for almost all cases, the measured O_4 dAMFs are systematically smaller than the simulated O_4 dAMFs. This is an important finding, because especially for the low elevation angles, the presence of aerosol scattering leads to a decrease of the O_4 dSCDs. Thus the

265   simulations for a pure Rayleigh atmosphere represent an upper limit of the achievable O_4 dSCDs. Only for cloudy cases with a high probability for multiple scattering events higher O_4 dSCDs could occur, but such conditions can be ruled out here because of the absence of thick and vertically extended clouds. Thus the overestimation of the simulated O_4 dSCDs for a pure Rayleigh atmosphere by the measured O_4 dSCDs indicates a fundamental inconsistency between measurements and simulations. Similar results are found for the elevation sequences with cloud contamination (Fig. A11 in the appendix).

270   In the right part of Fig. 6, simulation results for the aerosol profiles extracted in section 6.1 are shown. Note the separate y-axes for the simulated O_4 dAMFs on the right side, for which the maxima are chosen to achieve best agreement between the measured and simulated O_4 dAMFs. The exact values of the axis maxima were determined by fitting the measured O_4 dAMFs to the simulated O_4 dAMFs for elevation angles >4°. For these elevation angles the simulation results for the different profile shapes below 500m) are almost the same. Good qualitative agreement between measurements and

275   simulation is found, especially for the aerosol profiles with constant extinction below 500 m. However, the absolute values differ strongly. The ratios between measured and simulated O_4 dAMFs are found to bebetween 0.8 and 0.86. Again, similar results are found for the elevation sequences with cloud contamination (Fig. A11 in the appendix).

The scaling factors derived from this comparison between measured and simulated O_4 dSCDs are presented as blue data points in Fig. 7.

280

7.2 Profile inversion with MAPA

We also applied our profile inversion algorithm, the Mainz profile algorithm (MAPA, Beirle et al., 2019), to the measured O_4 dAMFs. For that purpose, a new MAPA LUT had to be created, because the lowest AOD in the original LUT (0.05) is

285   larger than all AODs observed on 2 May 2020. The new LUT includes AOD values from zero to 0.1 in steps of 0.02. MAPA provides the option to apply a fixed user-defined scaling factor, or to determine a scaling factor yielding best match between forward model and measurement during profile inversion.

In Fig. A12 in the appendix the retrieved extinction profiles are shown for different scaling factors. Here it should be noted that the individual measurements (not the sequences) with cloud contamination were skipped before the profile inversion.

290   Only profiles with either ‚valid' or ‚warning' flags are shown (profiles with ‚error' flags are not shown). In Fig. A13 in the appendix the retrieved AODs for the different scaling factors are compared to the tropospheric AODs from the sun photometer measurements (stratospheric AOD of 0.012 was subtracted). Also the RMS between the measured and simulated O_4 dAMFs are shown (right). The colour of the MAX-DOAS inversion results indicates the quality of the profile inversion.

Most valid profiles are obtained for scaling factors between 0.80 and 0.90, or for a free fitted (variable) scaling factor. For

295   the inversions with larger scaling factors, rather high RMS are found. For most cases, the retrieved AODs are smaller than those measured by the sun photometer. However, here it should be noted that for these low aerosol extinctions, the information content of the measurements is probably too low to constrain the aerosol extinction profiles, especially for high altitudes.

Atmospheric
Measurement
Techniques
Discussions

300 The obtained scaling factors are shown in Fig. 7. Overall good agreement between both comparison methods is found. For all elevation sequences, values of the scaling factor < 1 are found. For the direct comparison, the difference from unity is mostly larger than 15 % and can thus not be explained by the uncertainties of the measurements and simulations.

8 Conclusions

305

We compared measured and simulated O_4 absorptions for one day with very low aerosol optical depth. For such conditions, the uncertainties caused by imperfect knowledge of the aerosol properties play a smaller role than for comparison under more polluted conditions.

One important result of the comparison was that for all measurements, the observed O_4 absorption was higher than the
310 simulation results for an atmosphere without aerosols. In the absence of optically thick clouds, the simulated O_4 dAMFs for an atmosphere without aerosols constitutes an upper limit, since especially for the low elevation angles the inclusion of aerosols leads to a decrease of the O_4 absorption. The observed discrepancies thus indicate a fundamental inconsistency between simulations and measurements.

The measured O_4 absorptions are also compared to simulations including aerosol extinction profiles. The aerosol extinction
315 profiles were constrained by measurements of the sun photometer, the ceilometer and a climatology of stratospheric aerosols. Again, a large discrepancy was found for the absolute values. However, for the relative dependence of the O_4 dAMFs on the elevation angle good agreement could be achieved. For each elevation sequence, the ratio of simulated and measured O_4 dAMFs was calculated. For that purpose the elevation angles >4° were used, for which the O_4 dAMFs are almost insensitive to the profile shape in the lower atmospheric layers. For all elevation sequences, ratios of 0.85 or less were found. Similar
320 ratios were also obtained from the application of our profile inversion algorithm (MAPA) to the measurements. The observed discrepancies cannot be explained by the uncertainties of measurements and/or simulations. Here it is important to note that in the spectral analysis, we explicitly corrected for the (small) temperature dependence of the atmospheric O_4 absorption.

Our results indicate that something fundamental is missing/wrong in either the radiative transfer simulations or the spectral
325 analysis of the atmospheric O_4 absorptions. We did not find a clear reason for the discrepancies. One possible reason for the discrepancies could be a systematically too small O_4 absorption cross section.

Author contributions

330 T. Wagner performed the measurements, data analysis and prepared the manuscript. S. Dörner prepared the MAX-DOAS instrument and extracted the ERA interim data. S. Dörner and S. Donner contributed to the MAX-DOAS operation and data analysis. S. Beirle performed the MAPA profile inversions. S. Kinne operated the sun photometer and ceilometer.

Acknowledgements

335

Atmospheric
Measurement
Techniques
Discussions

References

345

Bogumil, K., J. Orphal, T. Homann, S. Voigt, P.Spietz, O.C. Fleischmann, A. Vogel, M. Hartmann, H. Bovensmann, J. Frerik and J.P. Burrows, Measurements of Molecular Absorption Spectra with the SCIAMACHY Pre-Flight Model: Instrument Characterization and Reference Data for Atmospheric Remote-Sensing in the 230-2380 nm Region, J. Photochem. Photobiol. A., 157, 167-184, 2003.

350 Beirle, S., Dörner, S., Donner, S., Remmers, J., Wang, Y., and Wagner, T.: The Mainz profile algorithm (MAPA), Atmos. Meas. Tech., 12, 1785–1806, https://doi.org/10.5194/amt-12-1785-2019, 2019.

Berrisford, P, Dee, DP, Poli, P, Brugge, R, Fielding, M, Fuentes, M, Kållberg, PW, Kobayashi, S, Uppala, S, Simmons, A, The ERA-Interim archive Version 2.0, ERA Report Series No.1 Version 2.0 (https://www.ecmwf.int/node/8174), 2011.

Chen, Z., Bhartia, P. K., Torres, O., Jaross, G., Loughman, R., DeLand, M., Colarco, P., Damadeo, R., and Taha, G.: 355 Evaluation of the OMPS/LP stratospheric aerosol extinction product using SAGE III/ISS observations, Atmos. Meas. Tech., 13, 3471–3485, https://doi.org/10.5194/amt-13-3471-2020, 2020.

Deutschmann, T., Beirle, S., Frieß, U., Grzegorski, M., Kern, C., Kritten, L., Platt, U., Pukite, J., Wagner, T., Werner, B., and Pfeilsticker, K.: The Monte Carlo Atmospheric Radiative Transfer Model McArtim: Introduction and Validation of Jacobians and 3D Features, J. Quant. Spectrosc. Ra., 112, 1119–1137, doi:10.1016/j.jqsrt.2010.12.009, 2011.

360 Donner, S.: Mobile MAX-DOAS measurements of the tropospheric formaldehyde column in the Rhein-Main region, Master's thesis, University of Mainz, http://hdl.handle.net/11858/00-001M-0000-002C-EB17-2, 2016.

Greenblatt G.D., Orlando, J.J., Burkholder, J.B., and Ravishankara, A.R.: Absorption measurements of oxygen between 330 and 1140 nm, J. Geophys. Res., 95, 18577-18582, 1990.

Hönninger, G. and Platt, U.: Observations of BrO and its vertical distribution during surface ozone depletion at Alert, 365 Atmospheric Environment, 36, 2481 – 2489, 2002.

Krastel, S., RV Maria S. Merian-Cruise MSM82/2, short cruise report, German Research Fleet Coordination Centre, University of Hamburg (https://www.ldf.uni-hamburg.de/merian/wochenberichte/wochenberichte-merian/msm82-2-msm84/msm82-2-scr.pdf), 2019.

Lampel, J., Pöhler, D., Polyansky, O. L., Kyuberis, A. A., Zobov, N. F., Tennyson, J., Lodi, L., Frieß, U., Wang, Y., Beirle, 370 S., Platt, U., and Wagner, T.: Detection of water vapour absorption around 363 nm in measured atmospheric absorption spectra and its effect on DOAS evaluations, Atmos. Chem. Phys., 17, 1271-1295, https://doi.org/10.5194/acp-17-1271-2017, 2017.

Ortega, I., Berg, L. K., Ferrare, R. A., Hair, J. W., Hostetler, C. A., and Volkamer, R.: Elevated aerosol layers modify the O_2-O_2 absorption measured by ground-based MAX-DOAS, J. Quant. Spectrosc. Ra., 176, 34–49, 375 https://doi.org/10.1016/j.jqsrt.2016.02.021, 2016.

Polyansky, O.L., A.A. Kyuberis, N.F. Zobov, J. Tennyson, S.N. Yurchenko and L. Lodi ExoMol molecular line lists XXX: a complete high-accuracy line list for water, Monthly Notices of the Royal Astronomical Society , 480 (2), 2597-2608, 2018.

Smirnov, A., B. N. Holben, I. Slutsker, D. M. Giles, C. R. McClain, T. F. Eck, S. M. Sakerin, A. Macke, P. Croot, G. 380 Zibordi, P. K. Quinn, J. Sciare, S. Kinne, M. Harvey, T. J. Smyth, S. Piketh, T. Zielinski, A. Proshutinsky, J. I. Goes, N. B. Nelson, P. Larouche, V. F. Radionov, P. Goloub, K. Krishna Moorthy, R. Matarrese, E. J. Robertson, and F. Jourdin Maritime Aerosol Network as a component of Aerosol Robotic Network, J. Geophys. Res., 114, D06204, doi:10.1029/2008JD011257, 2009.

Thalman, R. and Volkamer, R.: Temperature dependent absorption cross-sections of O_2–O_2 collision pairs between 340 and 385 630 nm and at atmospherically relevant pressure, Phys. Chem. Chem. Phys., 15, 15371, doi:10.1039/c3cp50968k, 2013.

Atmospheric
Measurement
Techniques
Discussions

Thomason, L. W., Ernest, N., Millán, L., Rieger, L., Bourassa, A., Vernier, J.-P., Manney, G., Luo, B., Arfeuille, F., and Peter, T.: A global space-based stratospheric aerosol climatology: 1979–2016, Earth Syst. Sci. Data, 10, 469–492, https://doi.org/10.5194/essd-10-469-2018, 2018.

Vandaele, A. C., C. Hermans, P. C. Simon, M. Carleer, R. Colin, S. Fally, M.-F. Mérienne, A. Jenouvrier, and B. Coquart,
390   Measurements of the NO2 Absorption Cross-section from 42000 cm-1 to 10000 cm-1 (238-1000 nm) at 220 K and 294 K, J. Quant. Spectrosc. Radiat. Transfer, 59, 171-184, 1997.

Wagner, T., Beirle, S., and Deutschmann, T.: Three-dimensional simulation of the Ring effect in observations of scattered sun light using Monte Carlo radiative transfer models, Atmos. Meas. Tech., 2, 113-124, 2009.

Wagner, T., Apituley, A., Beirle, S., Dörner, S., Friess, U., Remmers, J., and Shaiganfar, R.: Cloud detection and
395   classification based on MAX-DOAS observations, Atmos. Meas. Tech., 7, 1289-1320, doi:10.5194/amt-7-1289-2014, 2014.

Wagner, T., Beirle, S., Remmers, J., Shaiganfar, R., and Wang, Y.: Absolute calibration of the colour index and O_4 absorption derived from Multi AXis (MAX-) DOAS measurements and their application to a standardised cloud classification algorithm, Atmos. Meas. Tech., 9, 4803-4823, doi:10.5194/amt-9-4803-2016, 2016.

Wagner, T., Beirle, S., Benavent, N., Bösch, T., Chan, K. L., Donner, S., Dörner, S., Fayt, C., Frieß, U., García-Nieto, D.,
400   Gielen, C., González-Bartolome, D., Gomez, L., Hendrick, F., Henzing, B., Jin, J. L., Lampel, J., Ma, J., Mies, K., Navarro, M., Peters, E., Pinardi, G., Puentedura, O., Puķīte, J., Remmers, J., Richter, A., Saiz-Lopez, A., Shaiganfar, R., Sihler, H., Van Roozendael, M., Wang, Y., and Yela, M.: Is a scaling factor required to obtain closure between measured and modelled atmospheric O_4 absorptions? An assessment of uncertainties of measurements and radiative transfer simulations for 2 selected days during the MAD-CAT campaign, Atmos. Meas. Tech., 12, 2745–2817, https://doi.org/10.5194/amt-12-2745-
405   2019, 2019.

Wang, Y., Beirle, S., Hendrick, F., Hilboll, A., Jin, J., Kyuberis, A. A., Lampel, J., Li, A., Luo, Y., Lodi, L., Ma, J., Navarro, M., Ortega, I., Peters, E., Polyansky, O. L., Remmers, J., Richter, A., Puentedura, O., Van Roozendael, M., Seyler, A., Tennyson, J., Volkamer, R., Xie, P., Zobov, N. F., and Wagner, T.: MAX-DOAS measurements of HONO slant column densities during the MAD-CAT campaign: inter-comparison, sensitivity studies on spectral analysis settings, and error
410   budget, Atmos. Meas. Tech., 10, 3719-3742, https://doi.org/10.5194/amt-10-3719-2017, 2017.

Wang, Y., Apituley, A., Bais, A., Beirle, S., Benavent, N., Borovski, A., Bruchkouski, I., Chan, K. L., Donner, S., Drosoglou, T., Finkenzeller, H., Friedrich, M. M., Frieß, U., Garcia-Nieto, D., Gómez-Martín, L., Hendrick, F., Hilboll, A., Jin, J., Johnston, P., Koenig, T. K., Kreher, K., Kumar, V., Kyuberis, A., Lampel, J., Liu, C., Liu, H., Ma, J., Polyansky, O. L., Postylyakov, O., Querel, R., Saiz-Lopez, A., Schmitt, S., Tian, X., Tirpitz, J.-L., Van Roozendael, M., Volkamer, R.,
415   Wang, Z., Xie, P., Xing, C., Xu, J., Yela, M., Zhang, C., and Wagner, T.: Inter-comparison of MAX-DOAS measurements of tropospheric HONO slant column densities and vertical profiles during the CINDI-2 campaign, Atmos. Meas. Tech., 13, 5087–5116, https://doi.org/10.5194/amt-13-5087-2020, 2020.

420

425

430

435

Tables

Table 1: Settings for the DOAS analysis of O$_4$

Parameter	Value, Remark / Reference
Spectral range	352 – 387 nm
Degree of DOAS polynomial	5
Degree of intensity offset polynomial	2
Fraunhofer reference spectrum	Interpolated between 90° measurement before and after each elevation sequence
Wavelength calibration	Fit to high resolution solar spectrum using Gaussian slit function
Shift / squeeze	The measured spectrum is shifted and squeezed against all other spectra
Ring spectrum 1	Normal Ring spectrum calculated from measured zenith spectrum
Ring spectrum 2	Ring spectrum 1 multiplied by λ^{-4} (Wagner et al. (2009)
O$_3$ cross section	223 K, Bogumil et al. (2003)
NO$_2$ cross section	294 K, Vandaele et al. (1997)
H$_2$O cross section	293 K, Polyansky et al. (2018)
O$_4$ cross section	293 K, Thalman and Volkamer (2013)

440

Table 2: Vertical resolution used for the radiative transfer simulations

Altitude range [km]	Vertical resolution [km]
0 - 0.5	0.02
0.5 - 2	0.1
2 – 12	0.2
12 – 25	1
25 – 45	2
45 - 100	5

445

450

455

460

465

Figures

470
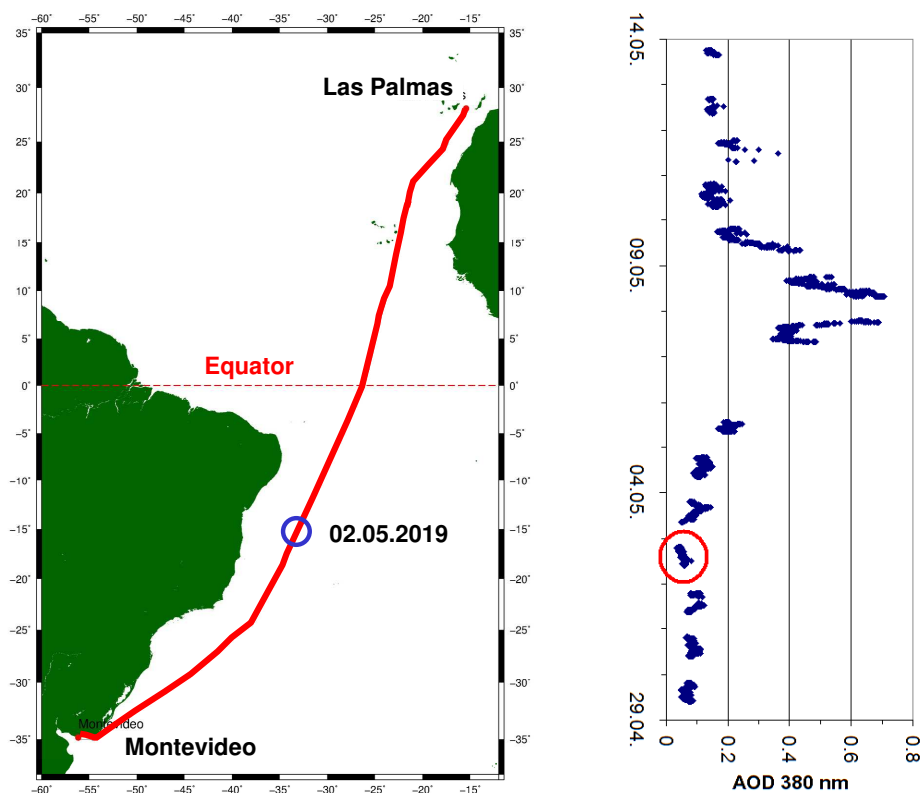
Fig. 1: Left: Ship route from Montevideo to Las Palmas. The blue circle indicates the location of the measurements used in this study. Right: Aerosol optical depth at 380 nm measured with a hand-held sun photometer.

475

480
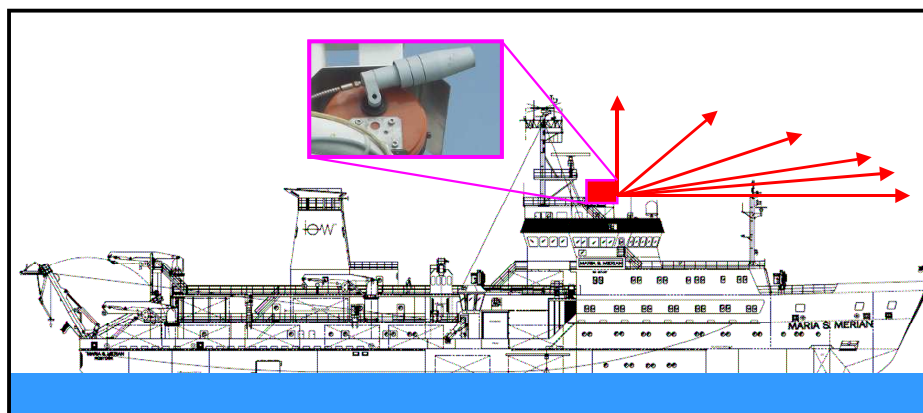
485 **Fig. 2: The position and viewing direction of the MAX-DOAS instrument on the RV Maria S. Merian during the ship cruise (ship drawing taken from https://briese-research.de/research-department/research-vessels/rv-maria-s-merian).**

490
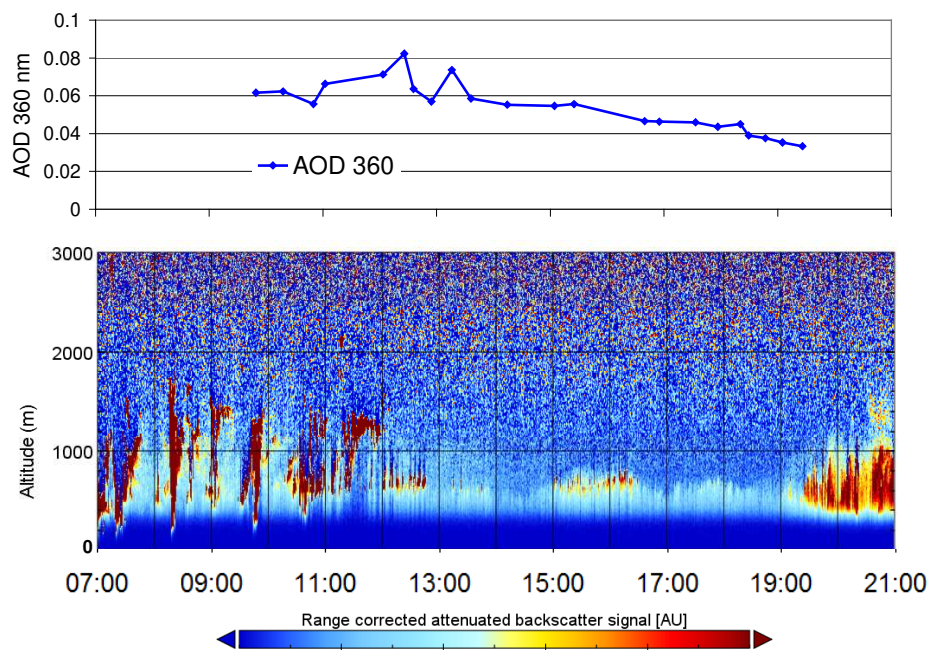
495 **Fig. 3: Top: AOD at 360 nm measured from the hand-held sun photometer. The data were extrapolated from the measurements at 380 nm using the Angström coefficient calculated from 380 nm and 440 nm. Bottom: Range-corrected ceilometer backscatter profile at 1064 nm.**

500
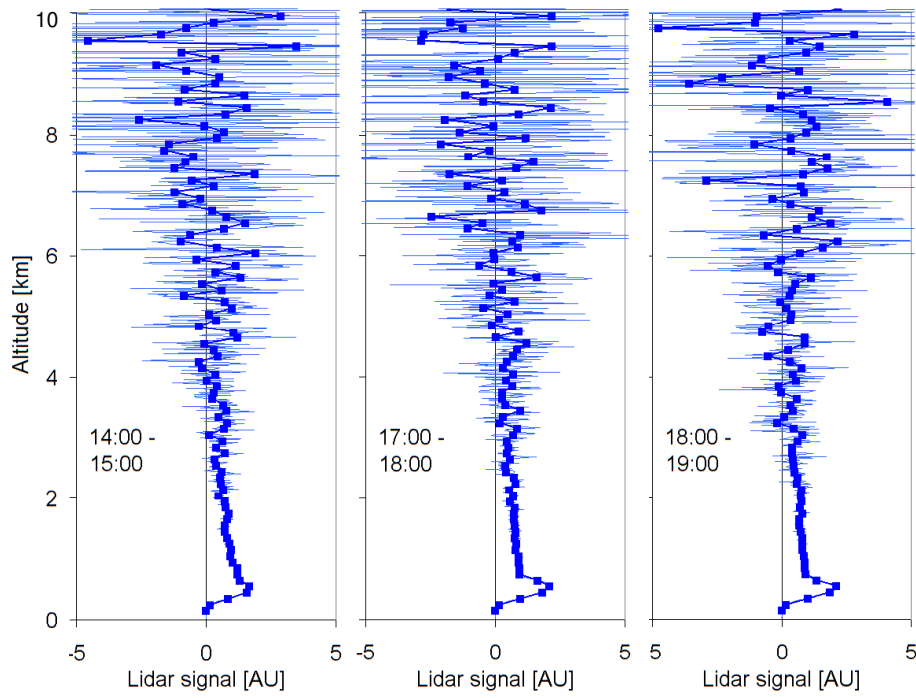
Fig. 4: Hourly averaged and range corrected ceilometer backscatter profiles for 3 periods on 2 May 2019 without cloud contamination. The thin lines represent the raw data. The dotted lines represent the smoothed profiles (averages over 100 m).
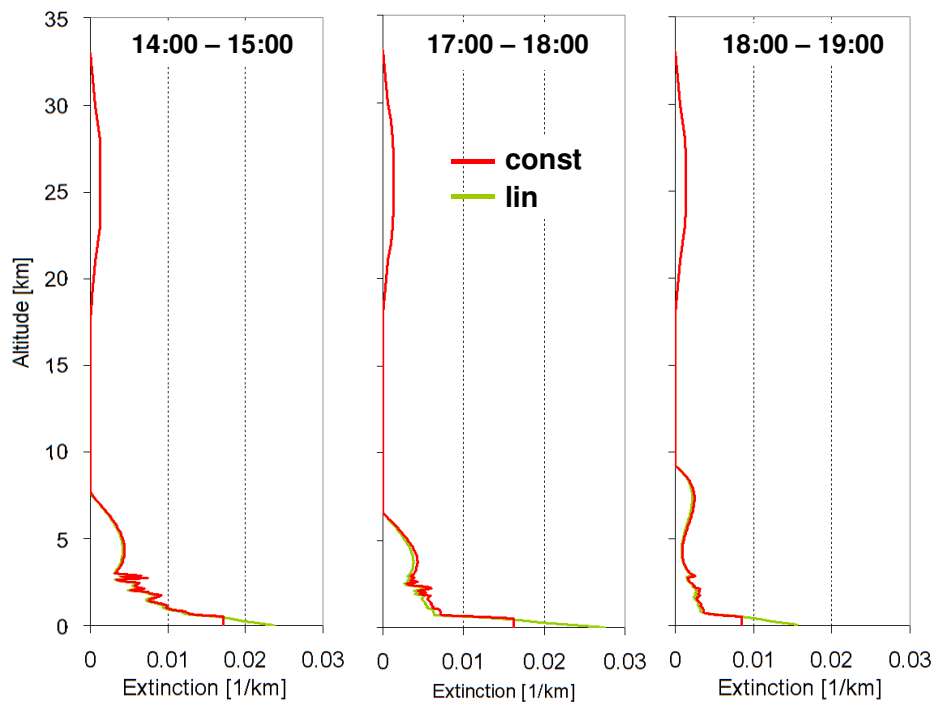
Fig. 5: Complete aerosol extinction profiles for the three time periods without clouds after all corrections are applied. The green curves represent the profiles with linear extrapolation below 500 m; the red curves represent profiles with constant values below 500 m.

Atmospheric
Measurement
Techniques
Open Access
Discussions
EGU

555
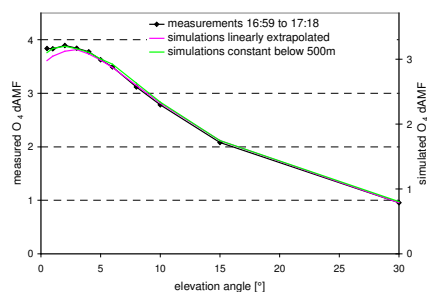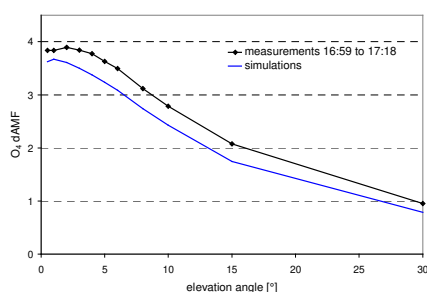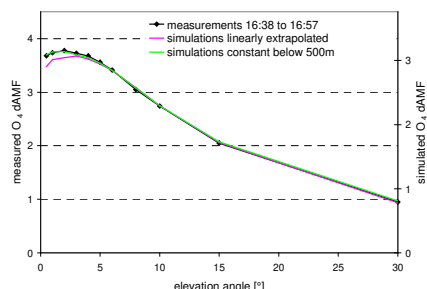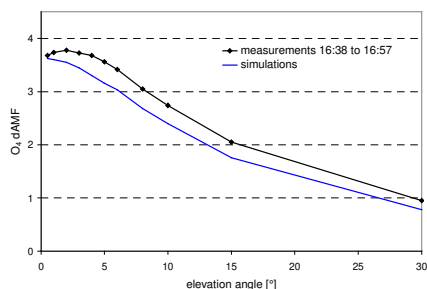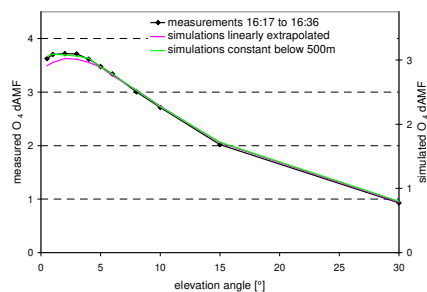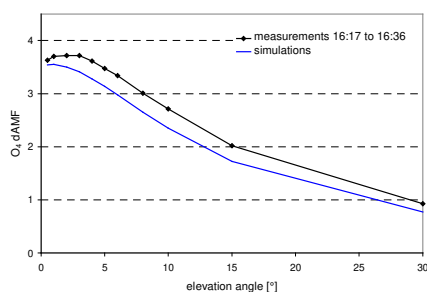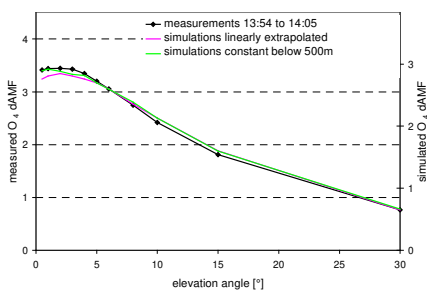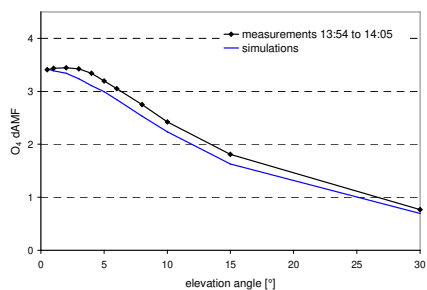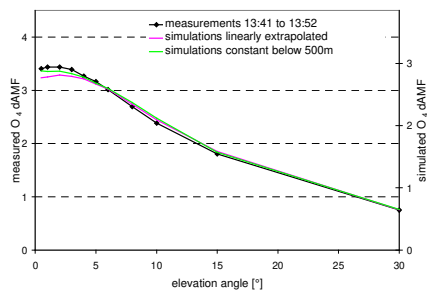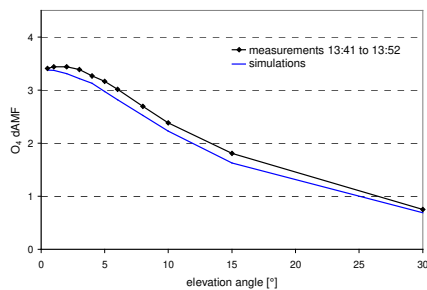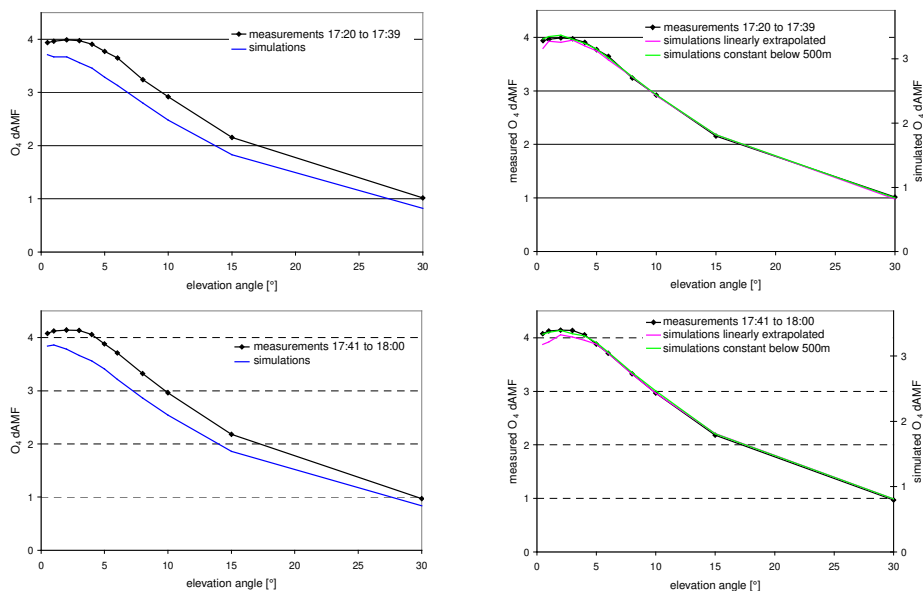
Fig. 6: Comparison of the measured and simulated O$_4$ dAMFs for selected elevation sequences without cloud contamination. In the left part, the measured O$_4$ dAMFs are compared to simulations for a pure Rayleigh atmosphere. In the right part they are compared to simulation results including aerosols (two profiles with either constant or linearly extrapolated aerosol extinction below 500 m). Note that in the right part separate y-axes on the right sides are used for the simulation results. The maxima of the right y-axes are chosen to achieve best agreement between the measured and simulated O$_4$ dAMFs (see text).
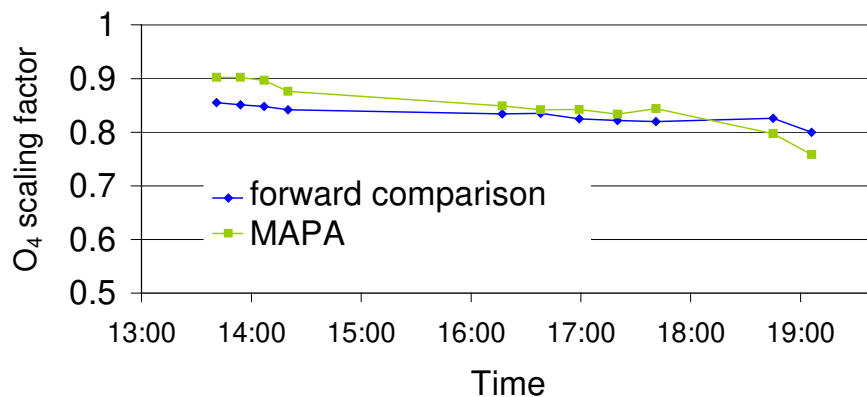
Fig. 7: Scaling factors derived from the direct comparison between the measured and simulated O$_4$ dSCDs (blue) and from the MAPA profile inversion (green) for all elevation sequences shown in Fig. 6 and Fig. A11. Many of the measurements of the two last elevation sequences are affected by clouds.

Appendix A1 Effect of including a H$_2$O cross section or a second O$_4$ cross section on the retrieved O$_4$ dSCDs

H$_2$O cross section

Recent studies found evidence for substantial atmospheric H$_2$O absorptions in measured spectra in the UV (Lampel et al., 2017, Wang et al., 2017, 2020). These absorptions are usually rather small, but especially for measurement conditions with high atmospheric humidity the inclusion of a H$_2$O cross section in the spectral analysis can be useful.

Fig. A1 presents examples of the spectral analysis with either a H$_2$O cross section included or excluded. A clear H$_2$O absorption signal is found around 363 nm. The H$_2$O dSCDs retrieved at 363 nm agree reasonably well (r²=0.63) with those retrieved at 442 nm (see Fig. A2) with a similar slope (2.07) as presented in Lampel et al. (2017) who found a slope of 2.39. If the H$_2$O cross section is not included in the analysis, a systematic structure appears in the residual. Thus, in this study, a water vapour cross section (Polyansky et al. 2018) is included in the spectral analysis. Here it should be noted that compared to other locations, the water vapour absorption during the ship cruise was rather high because most of the measurements were carried out under conditions of high atmospheric temperature and humidity. At other, colder locations, the impact of the H$_2$O absorption might be negligible.

Although the H$_2$O absorption is clearly found in the spectral analysis, the effect of including a H$_2$O cross section or not on the retrieved O$_4$ dSCDs is still rather small. If a H$_2$O cross section is included, the retrieved O$_4$ dSCDs are about 2.5 % larger than without a H$_2$O cross section included.

**O$_4$ cross section at low temperature**

We also investigated the effect of including a second O$_4$ cross section for low temperature (203 K). Before using this cross section in the fit it was orthogonalised with respect to the O$_4$ cross section at 293 K. Including the additional O$_4$ cross section leads to only small changes of the retrieved O$_4$ dSCD of about –1.5 %. Here it is interesting to note that the retrieved O$_4$ dSCDs for the O$_4$ cross section at low temperature were negative and the absolute values much smaller ($<2 \cdot 10^{43}$ molec^2/cm^5) than those at high temperature ($<6 \cdot 10^{43}$ molec^2/cm^5). The largest negative O$_4$ dSCDs for the O$_4$ cross section at low temperature were found indicating that the effective atmospheric temperatures decrease with elevation angle (see section 6.2). Also, the correlation between both O$_4$ dSCDs (r²=0.20) is very low. Thus we conclude that the measured spectra do not contain significant O$_4$ absorptions at low temperatures. For the interpretation of this finding it should be noted that low temperatures exist only at higher atmospheric layers. The O$_4$ absorptions at these layers mostly cancel out in the spectral analysis, because the light paths of the measured spectra and the Fraunhofer reference spectra at these layers are very similar. This explains that the retrieved O$_4$ absorptions at cold temperatures are very small. To further confirm this hypothesis, we calculated the effective temperatures for the O$_4$ absorptions on 2 May 2019 (see section 6.2) and found them to be very close to the temperature of the high temperature O$_4$ cross section (293 K). Based on these findings, the O$_4$ results in this study are retrieved without including a second O$_4$ cross section at low temperature. It should, however, be noted that for measurements at other locations and seasons including a second O$_4$ cross section in the spectral analysis might be meaningful.
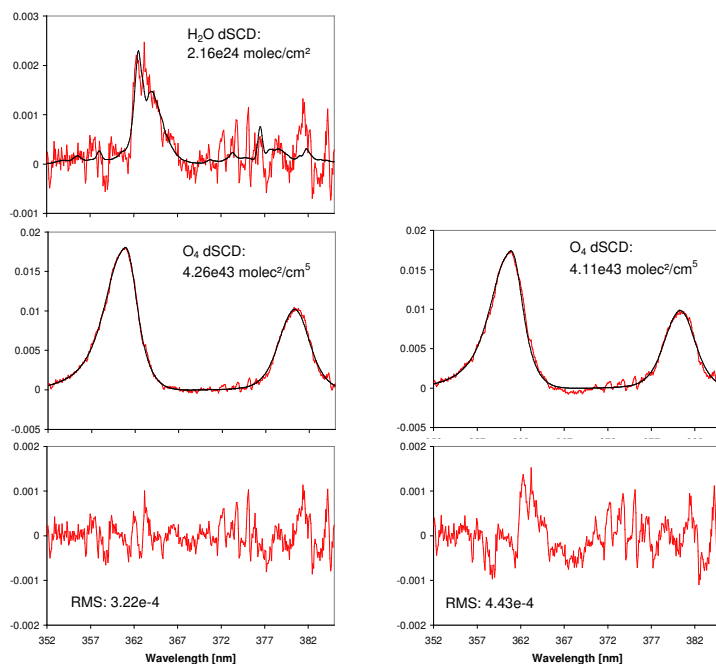
Fig. A1: Fit results for a spectrum taken on 2 May 2019, 13:14:50, at an elevation angle of 1° (SZA: 33.6°). Left: results if a H_2O cross section is included in the spectral analysis; right: results if no H_2O cross section is included in the spectral analysis. The black lines represent the fitted cross section, the red lines indicate the residual (bottom) or the residual plus the fitted cross section.
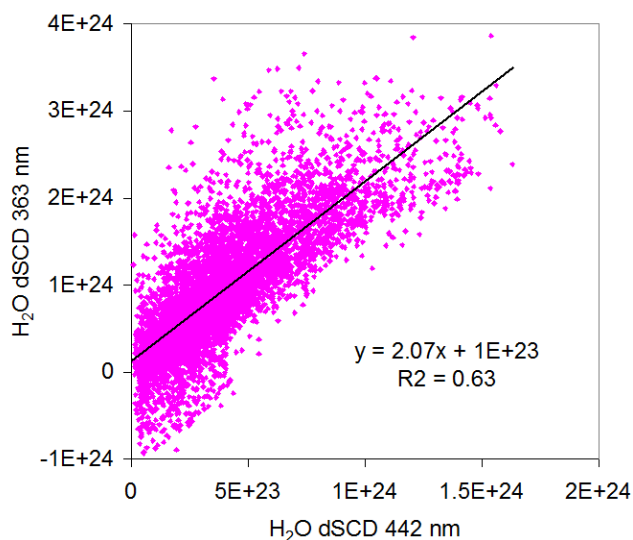

Fig. A2: Correlation plot of the H_2O dSCDs retrieved at 363 nm versus those retrieved at 442 nm for the whole ship cruise. The regression line is fitted assuming that the H_2O dSCDs retrieved at 442 nm have no error.

635

Appendix A2 Additional Figures

640
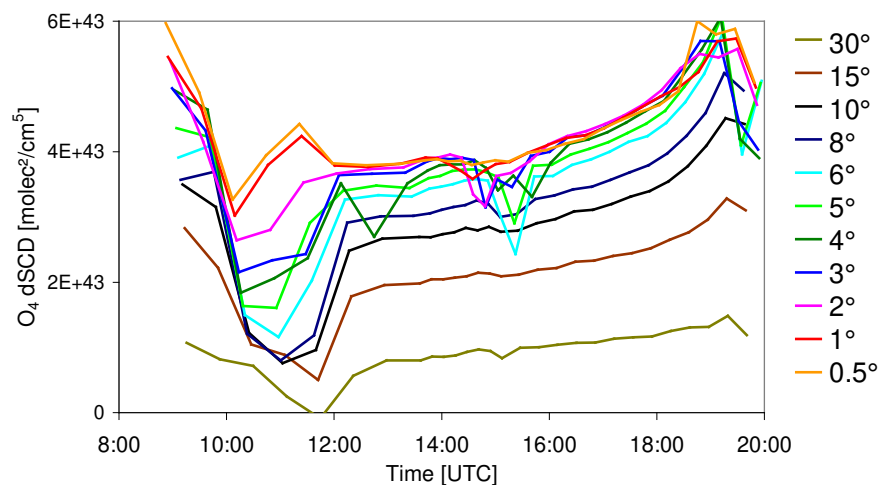
Fig. A3: Time series of the retrieved O$_4$ dSCD on 2 May 2019 for the different elevation angles. During the afternoon, for most of the time smooth variations are found. However, for some times and elevation angles systematic deviations of the O$_4$ dSCDs occur, which are caused by scattered clouds.

645
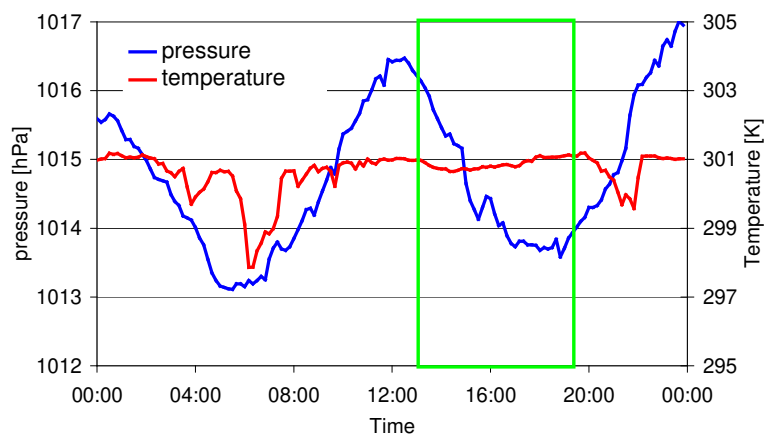
Fig. A4: Diurnal variation of the surface pressure and temperature from in situ measurements on the ship. The green
650 **box indicates the period of the MAX-DOAS measurements used in this study. The corresponding values from the ECMWF model simulations are 1012.8 hPa and 299.8 K, respectively.**
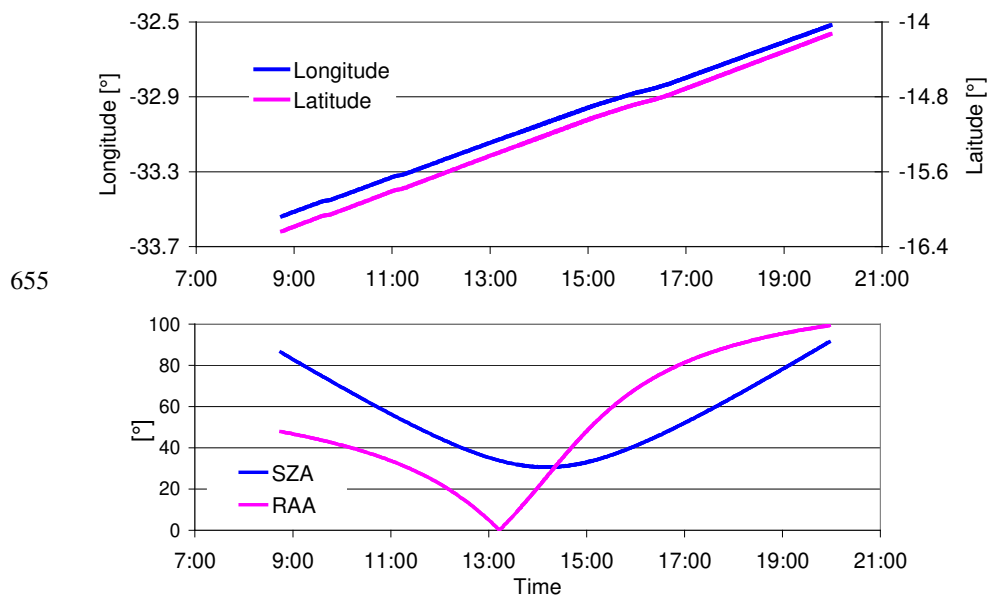
655

Fig. A5: Top: Variation of the latitude and longitude of the ship position during 2 May 2019. Bottom: Corresponding variation of the SZA and relative azimuth angle (RAA).

660
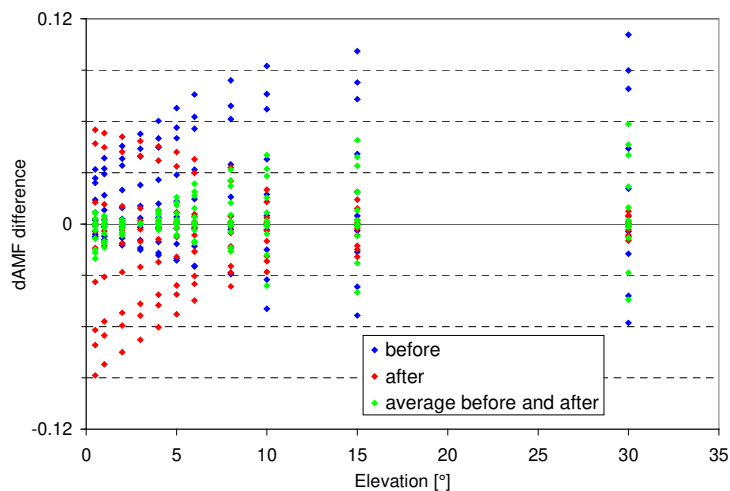
Fig. A6: Effect of using different Fraunhofer reference spectra for the analysis of individual elevation sequences. Shown are the ratios of the obtained O₄ dSCDs for different selections versus those for Fraunhofer reference spectra interpolated between the zenith measurements before and after the selected elevation sequence. Before: zenith

665 **measurent before the sequence is used; After: zenith measurent before the sequence is used; Average before and after: the average of the zenith measurents before and after the sequence is used.**
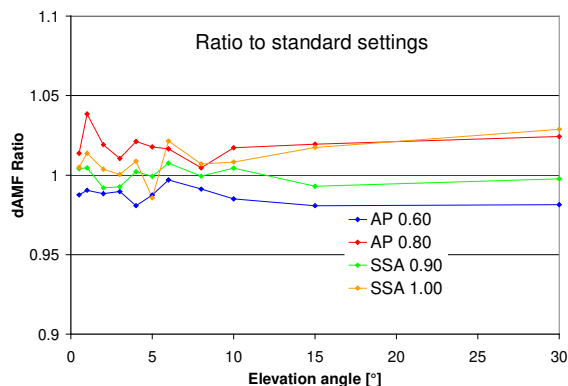
670

Fig. A7: Effect of different phase functions and single scattering albedos on the O$_4$ dSCDs. Shown are the ratios for simulations with variations of asymmetry parameter (AP) and single scattering albedo (SSA) versus simulations using the standard settings (AP= 0.68, SSA: 0.95). The results are for SZA of 64.5° and RAA of 87.7° (around 18:00 on 2 May 2019). The results for other SZA/RAA combinations during the afternoon of 2 May 2019 are similar.

675
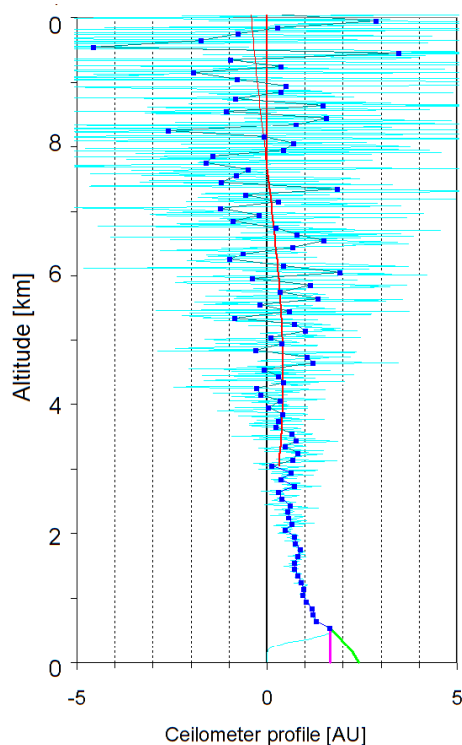
Fig. A8: The light blue data show the original backscatter profile averaged between 14:00 and 15:00. The blue dots show the smoothed (with a 100m kernel) profile, which are used between 500 m and 3 km. Below 500m either constant or linearly extraploated data (see tect) are used. Between 3 km and 10 km a third order polynomial is fitted
680 **to the raw data. The polynomial values are used between 3 km and the altitude at which they become negative. Above the values are set to zero.**

Atmospheric
Measurement
Techniques
Discussions
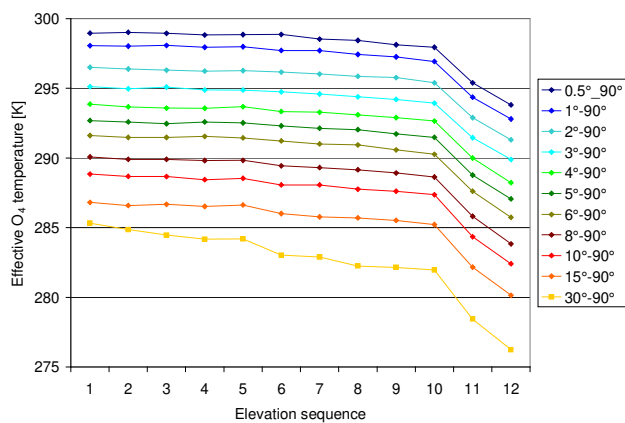
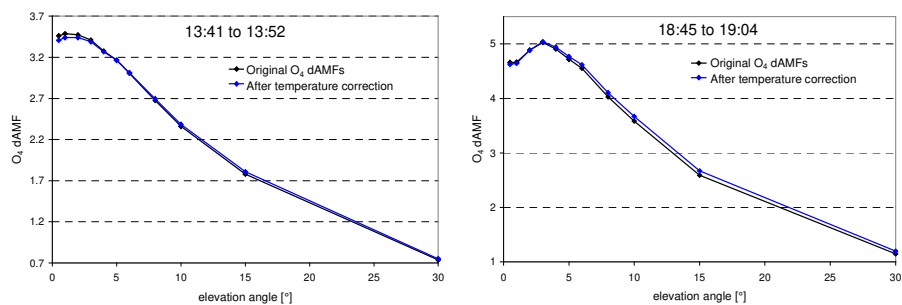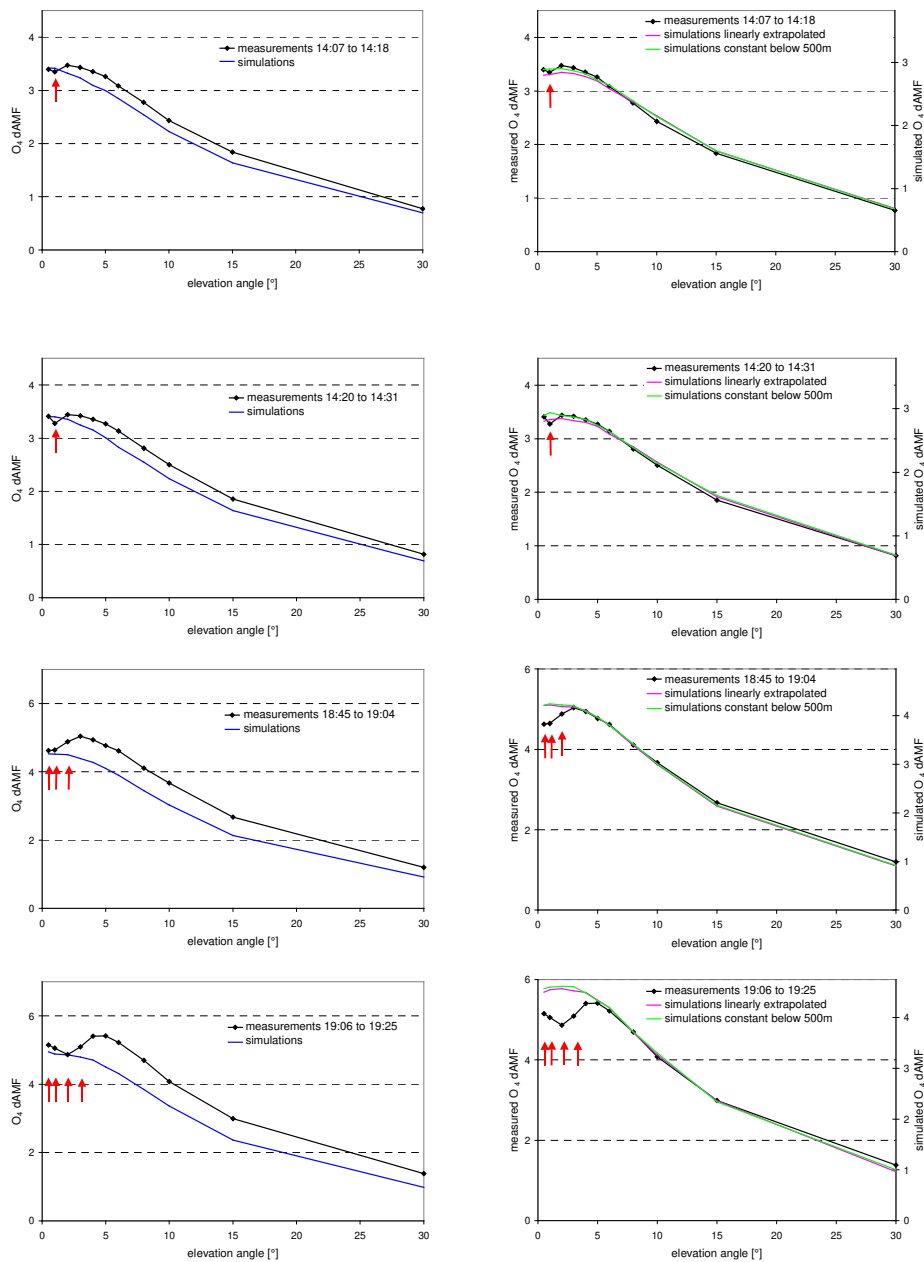Fig. A9: Effective temperatures calculated for the individual measurements according to equation 2.

Fig. A10: Effect of the temperature correction for two selected elevation sequences.

705

710

Fig A11: Comparison of the measured and simulated O$_4$ dAMFs for five elevation sequences with few cloud-contaminated measurements (indicated by the red arrows). In the left part, the measured O$_4$ dAMFs are compared to simulations for a pure Rayleigh atmosphere. In the right part they are compared to simulation results including

715 **aerosols (two profiles with either constant or linearly extraplolated aerosol extinction below 500 m). Note that in the right part separate y-axes on the right sides are used for the simulation results. The maxima of the right y-axes are chosen to achieve best agreement between the measured and simulated O$_4$ dAMFs (see text).**
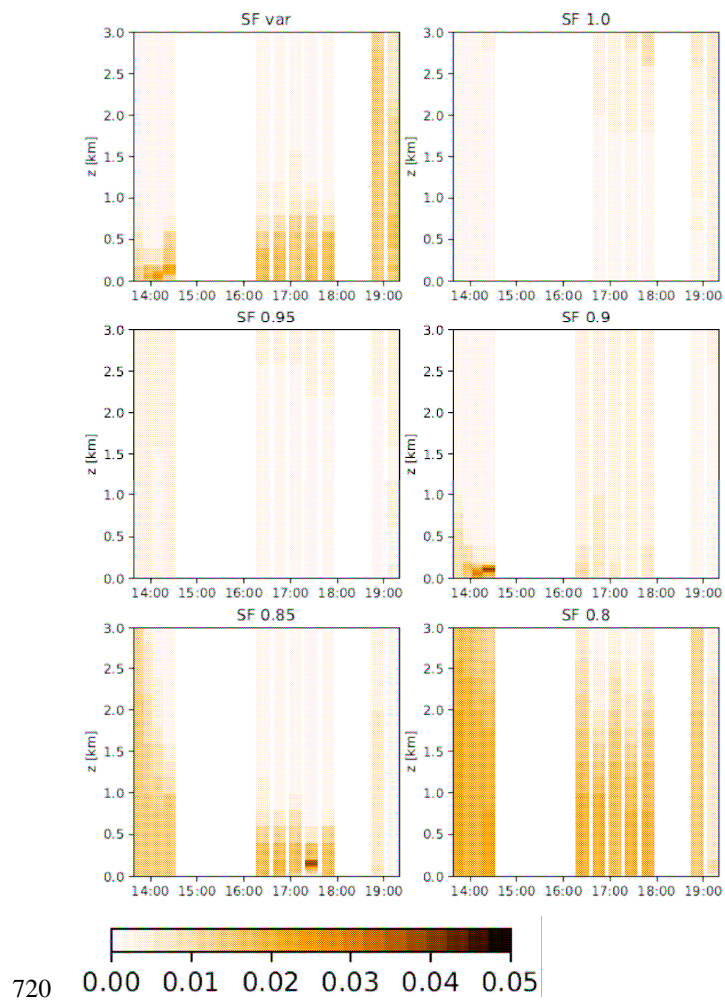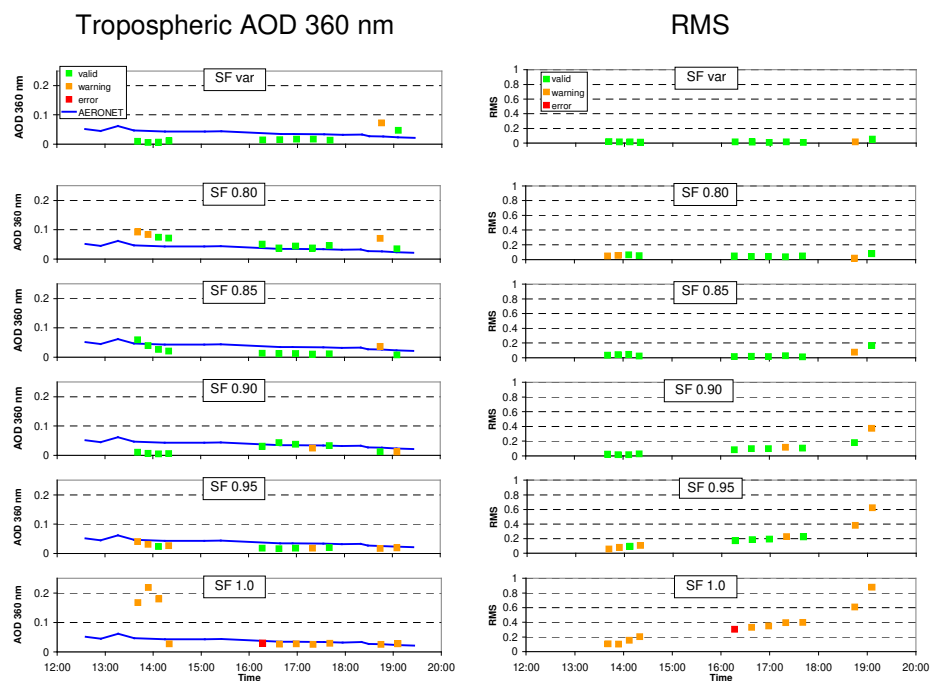
Fig A12: Extinction profiles retrieved with MAPA for the selected elevation sequences for different scaling factors. Only profiles for inversions with ‚valid' or ‚warning' flags are shown.

725

Fig A13: Right: Comparison of the retrieved AOD for the MAPA profile inversions with different scaling factors (squares) and the (tropospheric) AOD observed by the sun photometer (blue lines). **Right:** RMS between the measured and fitted O_4 dAMFs. The colours indicate the quality flags for the individual profile inversions.